Research Article | Vol. 27, No. 6 | 18 Mar 2019 | OPTICS EXPRESS 8011
Optics EXPRESS

Reduction of speckle noise and mitigation of beam wander in tunable external cavity quantum cascade lasers using rotating diamond/KBr pellet coupled with multimode fiber

YOHAN YOON,[1] CHRISTOPHER J. BRESHIKE,[1] CHRISTOPHER A. KENDZIORA,[2,*] ROBERT FURSTENBERG,[2] AND R. ANDREW MCGILL[2]

[1]American Society for Engineering Education Postdoctoral Fellow (residing at NRL), Washington, DC 20036, USA
[2]Naval Research Laboratory, Code 6365, 4555 Overlook Ave. SW, Washington, DC 20375, USA
[*]chris.kendziora@nrl.navy.mil

Abstract: We experimentally demonstrate speckle noise reduction and beam wander mitigation by using a rotating diamond/KBr pellet and a multimode fiber (MMF). As the diamond/KBr diffuser is rotated, the reflected speckle images that are captured by an infrared camera are temporally averaged. We demonstrate 78% speckle noise reduction by averaging 25 frames, which is within 80% of the theoretical contrast reduction. Large beam position fluctuations are also significantly suppressed by adding the MMF. This combination of beam wander mitigation and speckle reduction offers significant benefits for emerging optical technologies that use quantum cascade lasers as illumination sources.

1. Introduction

QCLs (quantum cascade lasers) have been an appealing light source for many applications, especially stand-off spectroscopy [1–4] and micro-spectroscopy [5,6] due to their high brightness and spectral range. However, a granular pattern called speckle is induced by the high degree of spatial coherence of the laser when it illuminates rough surfaces. This can interfere with attempts to image and detect small particles on planar surfaces. To discriminate analyte particles from the substrate, the speckle noise needs to be minimized. Extensive efforts have been made toward reducing the coherence of laser beams for suppressing speckle noise by utilizing diffractive optical elements [7–9], frequency compounding [10,11], multimode fibers (MMFs) [12–15], moving diffusers [16–19], and micro-electro-mechanical systems (MEMS) devices [20]. Here, we propose a facile method to fabricate a diamond/KBr pellet for use as a diffuser by pressing a mixture of potassium bromide (KBr) and diamond powders. The different refractive indexes of diamond and KBr in the pellet lead to phase variations generating a spatially incoherent laser source. As the diffuser is rotated, the speckle patterns in the reflected image from the rough surface of a sample illuminated by the laser source are temporally averaged. In this paper, we demonstrate that the rotating diamond/KBr diffuser reduces the speckle contrast significantly by temporal averaging.

Another serious issue with QCLs, especially external cavity (EC) QCLs, is beam wander induced by mode hops of the laser while the wavelength is swept for spectroscopic measurements such as stand-off detection techniques [21–23]. Any fluctuation of the laser beam direction out of the cavity and/or beam profile while the wavelength is swept results in a translation of the laser spot at the sample position. For a given pixel, this can often be misinterpreted as a spectral feature. As the distance between the laser and the target increases, this problem is amplified and could even result in some of the wavelengths of the laser

#357550 https://doi.org/10.1364/OE.27.008029
Journal © 2019 Received 14 Jan 2019; revised 12 Feb 2019; accepted 12 Feb 2019; published 4 Mar 2019

Optics EXPRESS

missing the target. If unaccounted for, this would lead to diminished performance (both in sensitivity and selectivity) of the detection technique. Beam wander is an important consideration for any detection technique requiring a small spot size to increase sensitivity. Here, we propose to couple the laser light into a MMF to suppress beam wander. The exit of the MMF acts as the new point source so that the wander is effectively mitigated.

In this study, we experimentally demonstrate a simplified optical configuration consisting of a rotating diamond/KBr diffuser and a MMF to reduce speckle noise and mitigate beam wander.

2. Fabrication and measurements setup

Commercially available diamond powders (natural diamond powder (NAT), Microdiamant) with two different particle diameter ranges (4 – 6 μm and 20 – 30 μm) were used in this study. Different mass loading levels (1 – 3%) of diamond powders for each particle size range were mixed with KBr powders. Pellets are pressed in a 13 mm die using 200 mg of diamond/KBr mixture. The pelletizing pressure was 517 MPa at ambient room temperature and held for 2 minutes. The final diamond/KBr pellet has a smooth surface with approximately 1 mm thickness. Figures 1(a) and 1(b) show optical images of diamond/KBr pellets made with two different mass loading levels of diamond powders, 1% and 2%, respectively. With the higher mass loading level of diamond powder (2%), the pellet is more opaque due to increased light scattering.

To quantify the transmittance of the laser beam through the diamond/KBr pellets, Fourier transform infrared spectroscopy (FTIR) transmittance spectra were collected, as shown in Fig. 1(c), with a Bruker Vertex V80 using a Pike diffuse reflectance attachment with the pellet mounted on a sample card in front of the integrating sphere. With the diffuse reflectance attachment, most of the transmitted light is collected, so the measured transmittance value is not the same as the amount of collected light through a ZnSe lens in the de-speckle setup which will be discussed in the following section. Note that the main purpose of the diffuse transmittance FTIR measurements is to compare the spectral throughput of different pellets with various mass loading levels and particle sizes, regardless of the amount of scatter.

As a reference, an FTIR spectrum of a KBr pellet is set as 100% transmittance. As expected, the transmittance of the pellet systematically decreases as the mass loading level of the diamond powder increases. For the pellet made with 20 – 30 μm diamond powders, the transmittance of the diamond pellet drops from 83% to 65% when the mass loading level of the diamond powders increases from 1% to 3%. Size of the diamond particles is also an important factor to determine the transmittance of the light through the pellet. For the same mass loading level, less light is collected through the pellet made using the smaller diamond particles. This is because for a given mass loading there are more small particles than large ones so there are more scattering centers for the incoming light to interact with. For the pellet with a mass loading level of 1% diamond, the transmittance drops from 83% to 62% when the particle size range is reduced from 20 – 30 μm to 4 – 6 μm. Note that none of the FTIR spectra show any spectral features, which is beneficial to spectroscopic techniques, such as stand-off detection of trace explosives [1,2]. The experimental results of the pellets with mass loading levels more than 3% of diamond and smaller particle sizes less than 4 – 6 μm are not included in this study since the transmittance of the laser light through those pellets are significantly lower. In these cases, transmission was too low to get adequate signal to noise ratio for the de-speckle studies described in the following section. Also, the experimental data of pellets with mass loading levels less than 1% of diamond are not included in this study since those pellets did not exhibit significant diffusion of the laser beam as characterized by a beam profiler (Pyrocam III, Ophir).

Optics EXPRESS

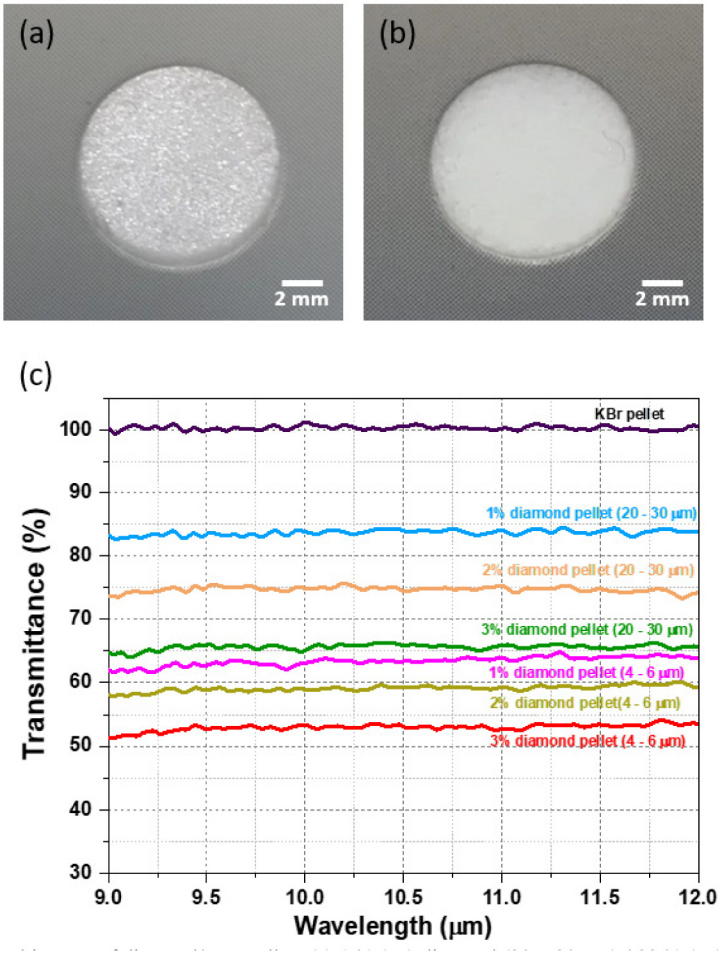

Fig. 1. Optical images of diamond/KBr pellets (a) 1% (wt) diamond (20 – 30 μm) / 99% (wt) KBr pellet and (b) 2% (wt) diamond (20 – 30 μm)/98% (wt) KBr pellet. (c) FTIR transmittance spectra for KBr pellet and 6 different diamond/KBr pellets with 1-3% (wt) loading level of diamond of two diamond size (20 – 30 μm, 4 – 6 μm) powders.

Figure 2 depicts schematics of the measurement setups with no diffuser or MMF and with the de-speckle unit. A tunable QCL (Daylight Solutions "MIRcat-QT") is employed as the active illumination source in Mid-LWIR range (6 – 11 μm in wavelength). The spectral width of the laser source is ~1 cm^{-1}. As shown in Fig. 2(a), without a de-speckle unit, the laser beam illuminates the surface of an Infragold disk directly and the diffusely reflected light is collected by an IR camera. To have the same beam path as the de-speckle configuration in Fig. 2(b), two protected gold mirrors are added. As a de-speckle setup, seen in Fig. 2(b), two off-axis parabolic (OAP) mirrors (33 mm reflected focal length) are used to couple the laser beam into a MMF and collimate the output beam from the MMF. A commercially available MMF (Newport, model 76908) was used in this study. This polycrystalline fiber has a 1 m length, a 400 μm core diameter, a 500 μm cladding diameter, and numerical aperture of (0.25. Coherent light from the QCL loses spatial coherence by passing through the MMF. The diamond/KBr pellet is placed in close proximity to the output of the OAP. The diamond/KBr pellet can be stationary or rotate at 4890 rpm (for comparison). The custom-built rotation stage is equipped with a motor, a bearing, and a 3D printed mount. The rpm value was measured using a commercially available tachometer. The laser beam transmitted through the

Optics EXPRESS

diffuser is re-collimated by a ZnSe collimation lens (12.7 mm focal length) having an anti-reflection coating for 3 – 12 μm and illuminates the surface of an Infragold disk. The diffusely reflected light is collected by an IR camera for the characterization of speckle noise. The IR camera was manufactured by Telops, it is a strained superlattice focal plane array with 30 μm pixels, and a 1000 mm f/2 lens was used focused about half a meter behind the target in order to emphasize the speckle features in the defocused image. The noise equivalent temperature difference (NETD) for the system is about 50 mK for these experiments. The frame rate of the camera is 300 Hz, and the frame integration time is 50 μs. The total power throughput of the "de-speckle" setup is measured using a photovoltaic IR sensor. The throughput efficiency of the de-speckle setup with a MMF and 1% diamond pellet (20 – 30 μm) is about 25%. The throughput efficiency drops to less than 10% when the mass loading of diamond is higher than 3% and the size range of diamond is smaller than 4 – 6 μm. The standoff distance from the collimation lens to the Infragold disk is approximately 400 mm. The spot size at the Infragold disk is approximately 12.6 mm.

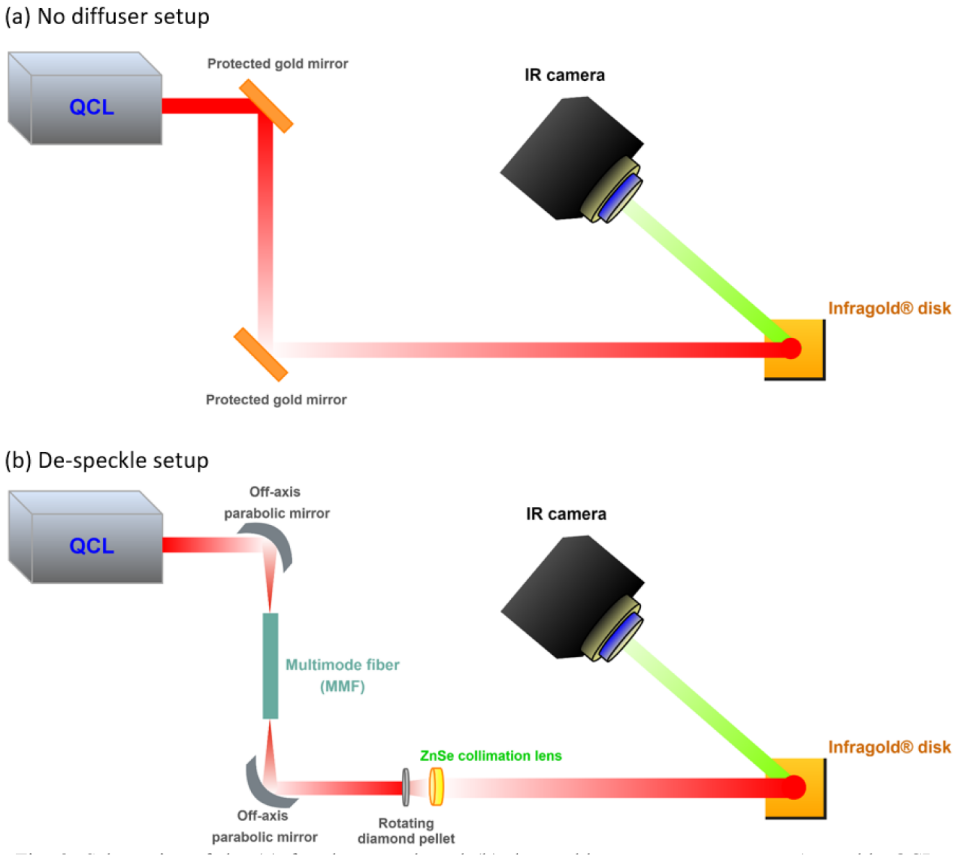

Fig. 2. Schematics of the (a) free beam path and (b) de-speckle measurement setup. A tunable QCL (Daylight Solutions "MIRcat-QT") is employed as the active illumination source. The laser light transmitted through either free beam path or de-speckle unit (multimode fiber and diamond/KBr diffuser) illuminates an Infragold disk, and the diffusely reflected light is collected by an IR camera for the characterization of speckle noise.

Optics EXPRESS

3. Results and discussion

3.1. Speckle reduction

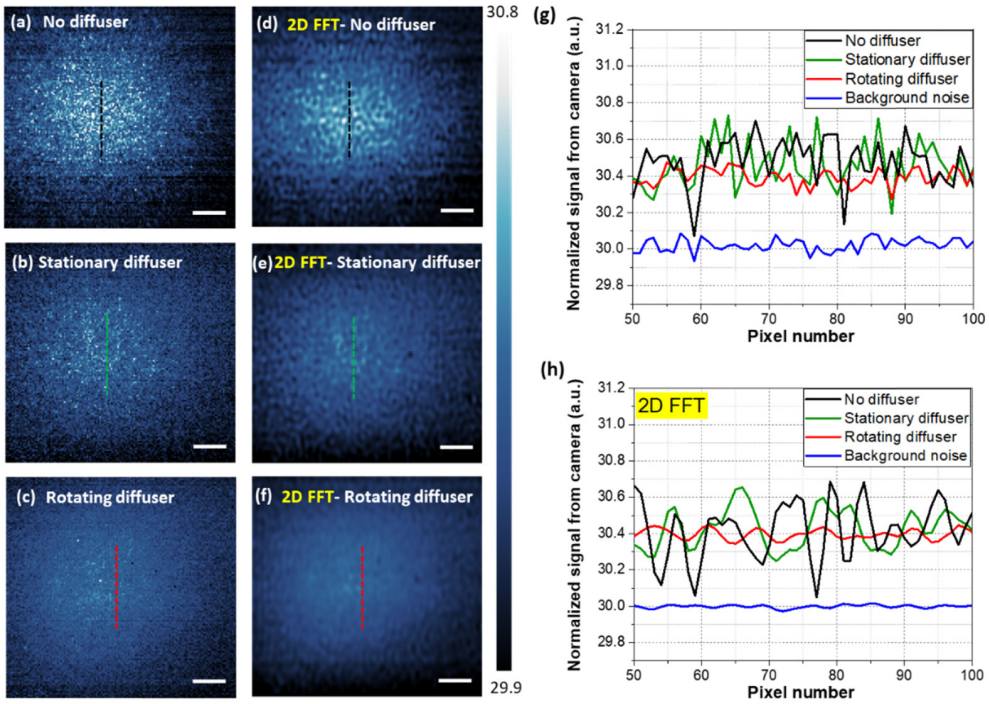

Fig. 3. Captured images with (a) no diffuser, (b) a stationary diffuser and (c) a rotating diffuser (1% mass loading level of 20 – 30 μm diamond). (g) Line profiles extracted from the dashed lines in the images show speckle intensity fluctuation. The intensities of the line profiles marked "No diffuser" are normalized for comparison. (d – f) 2D fast Fourier transform (FFT) filtered images of the raw captured images. (h) Line profiles extracted from the dashed lines in the 2D FFT filtered images show reduced signal noise levels. All scale bars in the captured images are 2 mm. The laser wavelength is 9 μm. The average power of the laser is 400 mW.

The reduction of the speckle led by temporal averaging of multiple frames using a diamond/KBr pellet is clearly seen in 2-dimensional (2D) images captured by an IR camera as shown in Fig. 3. With no diffuser, obvious speckle patterns are seen in the image in Fig. 3(a). Figure 3(b) shows a speckle image with a de-speckle setup by adding a MMF and a stationary diffuser (1% mass loading level of 20 – 30 μm diamond) illustrated in Fig. 2(b). A slight reduction of speckle noise is observed. More details of the experimental results of the pellets with higher mass loading levels (2% and 3%) of diamond will be discussed in the following section. As the diffuser is rotated, the speckle noise is greatly reduced by averaging multiple frames. Figure 3(c) shows an averaged speckle image from 25 temporally independent speckle images. This reduction of speckle noise is more clearly demonstrated in the line profile. Figure 3(g) shows line profiles extracted from the same area designated as dashed lines in each 2D speckle image and representative background noise extracted from a dark area in the same frame. Due to the laser intensity attenuation through the diamond/KBr diffuser, the signal intensities of the line profiles marked "No diffuser" in Figs. 3(g) and 3(h) are normalized for comparison. The fluctuation from the averaged signals (with 25 independent frames) is reduced by almost 75% when using the rotating diffuser compared to fluctuation with no diffuser.

As shown in Fig. 3(g), the background noise level is comparable to the 25 frames averaged signal using the rotating diffuser. To remove the sensor/camera noise from the

Optics EXPRESS

image, a 2D fast Fourier transform (FFT) was performed on each image. A low-pass filter (1000 m^{-1} cutoff frequency) is applied to the Fourier transform of the image, and the inverse transform is applied to obtain a filtered image which contains mainly the low-spatial frequency speckle noise. The 2D FFT filtered images in Figs. 3(d)–3(f) show suppressed sensor noise frequencies and discriminated speckle patterns. This is clearly shown in the line profile in Fig. 3h extracted from the same area designated as dashed lines in each 2D FFT filtered image. The background noise (blue line) is greatly suppressed so that each line profile shows discriminated speckle patterns.

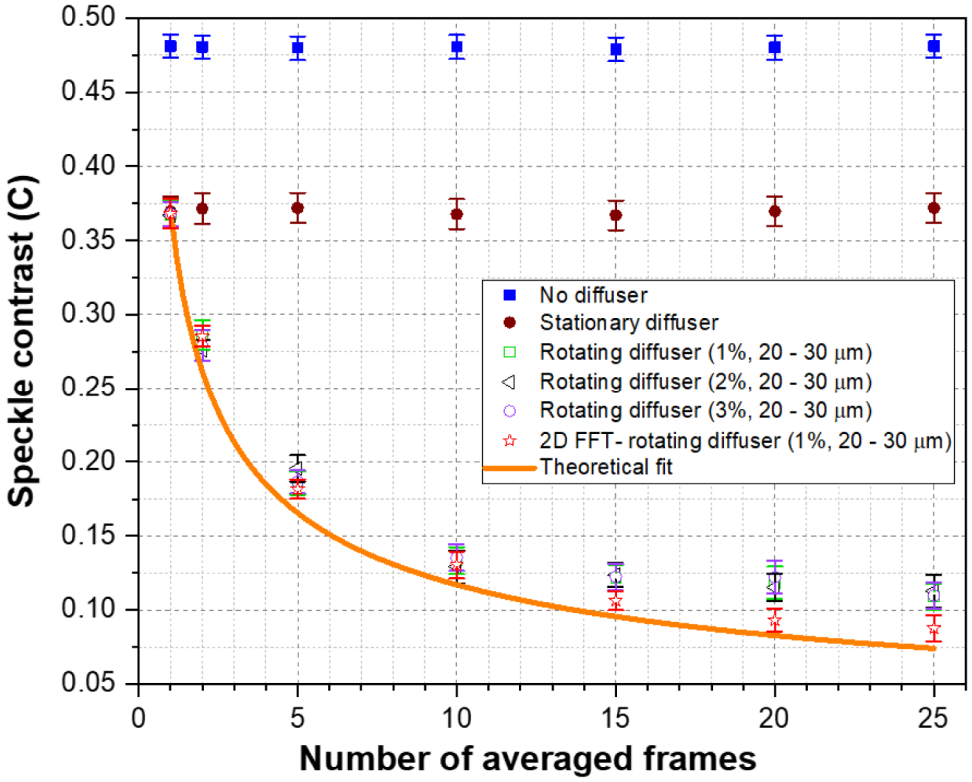

Fig. 4. The reduction of speckle contrast C extracted from speckle images as a function of the number of averaged frames with no diffuser, with a stationary, and three rotating diamond/KBr diffusers of different diamond mass loading levels (1 to 3%). The orange line represents the theoretical reduction of speckle contrast. The reduction of speckle contrast C extracted from speckle images with 2D FFT filtering (red star) as a function of the number of averaged frames using a rotating diamond/KBr diffuser (1% of 20 – 30 μm). The speckle contrast values extracted from 2D FFT filtered images are in better agreement with the theoretical reduction of speckle contrast (orange line).

We quantified the speckle reduction by calculating the speckle contrast C, which is defined as the ratio between the standard deviation σ_d and the mean intensity I_d [24],

$$C = \frac{\sigma_d}{I_d} \tag{1}$$

Fig. 4. shows the reduction of speckle contrast as a function of the number of averaged frames. The speckle contrast was extracted from the diffusely reflected images with and without the de-speckle setup. The uncertainty reported here is a single standard deviation of speckle contrasts extracted from various line profiles within the captured image. The speckle contrast without the diffuser extracted from the image in Fig. 3(a) is 0.48. The speckle

Optics EXPRESS

contrast decreases to 0.38 in the de-speckle setup with a stationary diamond/KBr diffuser. The speckle contrast for the "no diffuser" and the "stationary diffuser" show almost the same values with averaging multiple frames as shown in Fig. 4. This is expected as the speckle pattern is not changing significantly between frames when the diffuser is not moving. Therefore, averaging these frames only removes the background noise, not the deviations caused by speckle.

As the diffuser is rotated, every point on the object experiences a changing phase of illumination. Therefore, the speckle patterns of the diffusely reflected image change with time. The speckle contrast for three diamond/KBr pellets with different mass loading levels from 1 to 3% of 20 – 30 μm diameter diamond powders are determined. As expected, the reduction of speckle contrast with temporal averaging is observed. The speckle contrast of 1% diamond diffuser is rapidly reduced by 57% from 0.37 to 0.16 with averaging of 5 frames and then the speckle contrast slowly decreases to around 0.11 with averaging 25 independent speckle images. The 2% and 3% diamond diffusers have similar tendency of the speckle reduction with temporal averaging to that of 1% diamond diffuser. The speckle contrast values are slightly different from each other, but they are all within the error ranges. As mentioned previously, diamond pellets with less than 1% mass loading level do not exhibit significant diffusion and therefore were not implemented. This implies that mass loading less than 1% is not sufficient to generate independent speckle patterns. Once the mass loading level reaches 1%, the diamond diffuser is effective enough to reduce the speckle contrast with temporal averaging. Higher diamond content in the diffuser is not beneficial for the reduction of speckle as it only reduces the transmittance of light as shown in Fig. 1.

The theoretical contrast reduction of temporally integrated speckle is given by

$$C \propto \frac{1}{\sqrt{M}} \tag{2}$$

where M is the number of independent speckle patterns with equal mean intensities [16,24]. The orange solid line in the Fig. 4 represents the theoretical reduction of speckle contrast according to the $\sqrt{M}$ rate. The trend of the theoretical line shows very good agreement with the experimental results. The experimental values of speckle contrast are slightly higher than the theoretical values as the M value increases. Note that this is because the speckle patterns are not completely independent [10].

The effect of 2D FFT filtering on reduction of speckle contrast is shown in Fig. 5. As seen in Eq. (1), standard deviation is the main term to determine speckle contrast. The total standard deviation (σ_T of signal is contributed by standard deviation of sensor noise (σ_N) and standard deviation of speckle (σ_S) as expressed in Eq. (3).

$$\sigma_T = \sqrt{\sigma_N{}^2 + \sigma_S{}^2} \tag{3}$$

The speckle contrast C of the stationary diffuser and "no diffuser" do not change with performing 2D FFT filtering since the contribution of σ_N to σ_T is negligible when σ_S is much larger than σ_N . However, when σ_S is reduced with averaging frames, σ_S becomes comparable to σ_N . In this case, speckle contrast is also affected by background noise. Thus, the separation of noise in the averaged signal by performing 2D FFT filtering lowers speckle contrast. Figure 4 shows the reduction of speckle contrast with 2D FFT filtering (red star). The speckle contrast values with 2D FFT filtering are almost the same up to 5 averaged frames, and start deviating from the original values upon averaging additional frames. Note that the speckle contrast values extracted from 2D FFT filtered images are in better agreement with the theoretical values.

Optics EXPRESS

3.2. Mitigation of beam wander

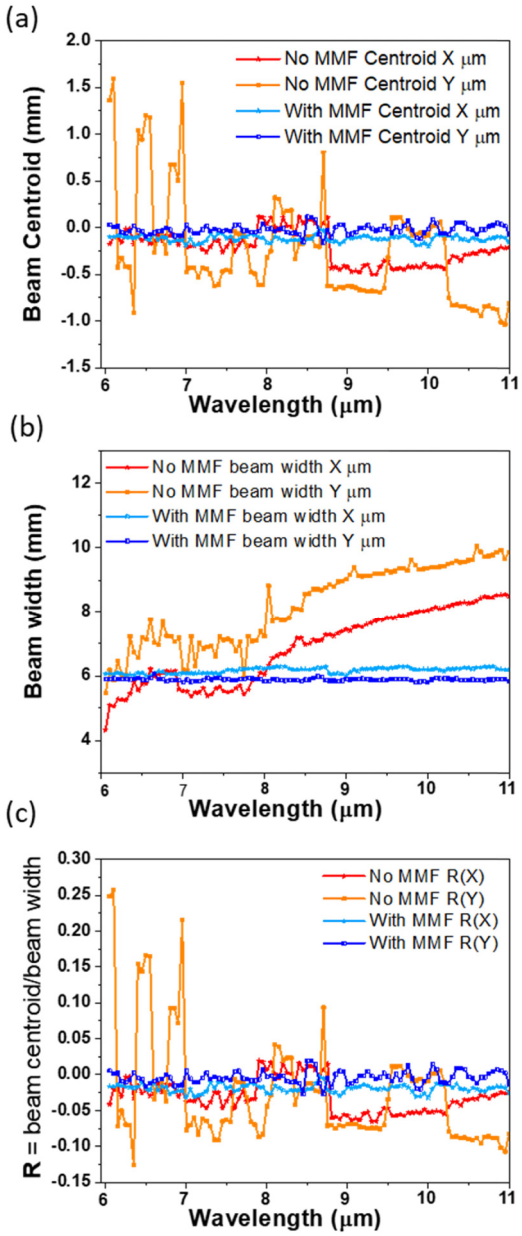

Fig. 5. (a) Beam centroid (X and Y), (b) Beam widths (X and Y). (c) Ratio (R) of beam centroid to beam width.

As an active illumination source, the wavelength of the tunable QCL is swept from 6 to 11 μm at a rate of 0.05 μm/s in continuous wave (CW) mode. The beam wander is characterized by measuring beam center position using a commercial beam profiler (Pyrocam III, Ophir). The optical setup is the same as the de-speckle configuration shown in Fig. 2(b), except that the beam profiler replaces the Infragold disk. The standoff distance from the collimation lens to the beam profiler is approximately 400 mm.

Optics EXPRESS

Figure 5 shows the beam centroid (a), beam width (b) in X and Y coordinates with no MMF and with the MMF and the diamond/KBr diffuser (1% mass loading level of 20 – 30 μm diamond). Without MMF, the extensive fluctuations in both beam position and width in both X (red line) and Y (orange line) directions are observed. Note that these fluctuations would lead to diminished performance (both in sensitivity and false alarms), which is not suitable for any detection technique, such as stand-off spectroscopy. These fluctuations in both beam position and beam width are significantly suppressed in both X and Y directions by adding a MMF. Note that beam centroid and beam width values change with the stand-off distance. Thus, the ratio (R) between beam centroid and beam width needs to be considered. Figure 5(c) shows the fluctuation of R from 6 to 11 μm. Even though the small fluctuation of R with the MMF exists, the R values are quite stable over the entire wavelength range from 6 to 11 μm. The improvement in laser beam pointing stability using the MMF in the de-speckle setup is also demonstrated.

4. Conclusion

In summary, diamond/KBr pellets acting as diffusers were fabricated by pressing a mixture of KBr powders with different mass loading levels of diamond powders of various particle sizes. The reduction of speckle noise and mitigation of beam wander using diamond/KBr pellets and multimode fiber were characterized using a de-speckle set-up consisting of a tunable QCL, Infragold disk, and IR camera. The diffusely reflected 2D speckle images from the surface of an Infragold disk clearly show the trend of speckle reduction with temporal averaging. The total power throughput of the "de-speckle" setup using a multimode fiber and 1% diamond pellet (20 – 30 μm) is about 25% measured using a photovoltaic IR sensor. Speckle contrast is slightly reduced with a multimode fiber and a stationary diffuser. As the diffuser is rotated, speckle noise is significantly suppressed with temporal averaging of multiple independent speckle images. The 2D FFT filtered images show suppressed sensor noise frequencies and discriminated speckle patterns. The experimental evidence for the speckle reduction (78% reduction) is in good qualitative agreement with the theoretical model (80% reduction). The diffuser and the multimode fiber were also leveraged to mitigate beam wander while the wavelength is swept for a spectroscopic measurement. To document this, the beam wander was characterized using a beam profiler. Large fluctuations in the beam position and width in both X and Y centroids were observed with no multimode fiber. These fluctuations were greatly suppressed by adding a multimode fiber. We believe that the proof of concepts presented here have broad applicability. These will aid in laser speckle and beam wander reduction, leading to more effective laser illumination for applications such as spectroscopy, imaging, and chemical detection.

Funding

Office of Naval Research/Naval Research Laboratory base program (63-1C33).

Acknowledgments

The authors thank Heungsoo Kim for fruitful discussion about pelletizing.

References

1. C. A. Kendziora, R. Furstenberg, M. Papantonakis, V. Nguyen, J. Byers, and R. Andrew McGill, "Infrared photothermal imaging spectroscopy for detection of trace explosives on surfaces," Appl. Opt. **54**(31), F129–F138 (2015).
2. R. Furstenberg, C. A. Kendziora, J. Stepnowski, S. V. Stepnowski, M. Rake, M. R. Papantonakis, V. Nguyen, G. K. Hubler, and R. A. McGill, "Stand-off detection of trace explosives via resonant infrared photothermal imaging," Appl. Phys. Lett. **93**(22), 224103 (2008).
3. F. Fuchs, B. Hinkov, S. Hugger, J. M. Kaster, R. Aidam, W. Bronner, K. Köhler, Q. Yang, S. Rademacher, K. Degreif, F. Schnürer, and W. Schweikert, "Imaging stand-off detection of explosives using tunable MIR quantum cascade lasers," in Quantum Sensing and Nanophotonic Devices VII (Vol. 7608, p. 760809) (2010).

Optics EXPRESS

4. M. F. Witinski, R. Blanchard, C. Pfluegl, L. Diehl, B. Li, K. Krishnamurthy, B. C. Pein, M. Azimi, P. Chen, G. Ulu, G. Vander Rhodes, C. R. Howle, L. Lee, R. J. Clewes, B. Williams, and D. Vakhshoori, "Portable standoff spectrometer for hazard identification using integrated quantum cascade laser arrays from 6.5 to 11 μm," Opt. Express **26**(9), 12159–12168 (2018).
5. R. Furstenberg, C. A. Kendziora, M. R. Papantonakis, V. Nguyen, and R. A. McGill, "Chemical imaging using infrared photothermal microspectroscopy," Proc. SPIE **8374**, 837411 (2012).
6. A. Hasenkampf, N. Kröger, A. Schönhals, W. Petrich, and A. Pucci, "Surface-enhanced mid-infrared spectroscopy using a quantum cascade laser," Opt. Express **23**(5), 5670–5680 (2015).
7. T. Tschudi, "Speckle reduction in laser projections with ultrasonic waves," Opt. Eng. **39**(6), 1659–1664 (2000).
8. G. Ouyang, Z. Tong, M. N. Akram, K. Wang, V. Kartashov, X. Yan, and X. Chen, "Speckle reduction using a motionless diffractive optical element," Opt. Lett. **35**(17), 2852–2854 (2010).
9. W. F. Hsu and C. F. Yeh, "Speckle suppression in holographic projection displays using temporal integration of speckle images from diffractive optical elements," Appl. Opt. **50**(34), H50–H55 (2011).
10. C. Magnain, H. Wang, S. Sakadžić, B. Fischl, and D. A. Boas, "En face speckle reduction in optical coherence microscopy by frequency compounding," Opt. Lett. **41**(9), 1925–1928 (2016).
11. G. E. Trahey, J. W. Allison, S. W. Smith, and O. T. von Ramm, "A quantitative Approach to Speckle Reduction via Frequency Compounding," Ultrason. Imaging **8**(3), 151–164 (1986).
12. D. S. Mehta, D. N. Naik, R. K. Singh, and M. Takeda, "Laser speckle reduction by multimode optical fiber bundle with combined temporal, spatial, and angular diversity," Appl. Opt. **51**(12), 1894–1904 (2012).
13. A. Efimov, "Coherence and speckle contrast at the output of a stationary multimode optical fiber," Opt. Lett. **43**(19), 4767–4770 (2018).
14. B. Redding, G. Allen, E. R. Dufresne, and H. Cao, "Low-loss high-speed speckle reduction using a colloidal dispersion," Appl. Opt. **52**(6), 1168–1172 (2013).
15. R. Furstenberg, C. A. Kendziora, C. J. Breshike, V. Nguyen, and R. A. McGill, "Laser speckle reduction techniques for mid-infrared microscopy and stand-off spectroscopy. in Next-Generation Spectroscopic Technologies X (Vol. 10210, p. 1021004) (2017).
16. S. Kubota and J. W. Goodman, "Very efficient speckle contrast reduction realized by moving diffuser device," Appl. Opt. **49**(23), 4385–4391 (2010).
17. G. Li, Y. Qiu, and H. Li, "Coherence theory of a laser beam passing through a moving diffuser," Opt. Express **21**(11), 13032–13039 (2013).
18. J. Lehtolahti, M. Kuittinen, J. Turunen, and J. Tervo, "Coherence modulation by deterministic rotating diffusers," Opt. Express **23**(8), 10453–10466 (2015).
19. B. Hinkov, F. Fuchs, J. M. Kaster, Q. Yang, W. Bronner, R. Aidam, and K. Köhler, "Broad band tunable quantum cascade lasers for stand-off detection of explosives," in J. C. Carrano and C. J. Collins, eds. (International Society for Optics and Photonics), Vol. 7484, p. 748406 (2009).
20. T.-K.-T. Tran, S. Subramaniam, C.-P. Le, S. Kaur, S. Kalicinski, M. Ekwinska, E. Halvorsen, and M. N. Akram, "Design, Modeling, and Characterization of a Microelectromechanical Diffuser Device for Laser Speckle Reduction," J. Microelectromech. Syst. **23**(1), 117–127 (2014).
21. C. J. Breshike, C. A. Kendziora, R. Furstenberg, V. Nguyen, and R. A. McGill, " "Stabilizing infrared quantum cascade laser beams for standoff detection applications." in Quantum Sensing and Nano Electronics and Photonics XIV, vol. 10111, p. 101110B. (2017).
22. R. Müller, C. A. Kendziora, and R. Furstenberg, "Feedback stabilization of quantum cascade laser beams for stand-off applications," in In Micro-and Nanotechnology Sensors. Systems, and Applications IX **10194**, 101942U (2017).
23. R. Furstenberg, C. A. Kendziora, M. R. Papantonakis, V. Nguyen, and R. A. McGill, "Characterization and control of tunable quantum cascade laser beam parameters for stand-off spectroscopy," in Chemical, Biological, Radiological, Nuclear, and Explosives (CBRNE) Sensing XVII (Vol. 9824, p. 98240L) (2016).
24. J. W. Goodman, Speckle Phenomena in Optics: Theory and Applications (Roberts & Company, 2007).